



Impulsive loading of clamped monolithic and sandwich beams over a central patch

X. Qiu, V.S. Deshpande*, N.A. Fleck

Cambridge University Engineering Department, Trumpington Street, Cambridge, CB2 1PZ, UK

Received 3 May 2004; received in revised form 15 November 2004; accepted 29 December 2004

Abstract

An analytical model is developed for the response of clamped monolithic and sandwich beams subjected to impulse loading over a central loading patch. A number of topologies of sandwich core are investigated, including the honeycomb core, pyramidal core, prismatic diamond core and metal foam. The various cores are characterised by their dependencies of through-thickness compressive strength and longitudinal tensile strength upon relative density. Closed-form expressions are derived for the deflection of the beam when the ratio r of length of loading patch to the beam span exceeds 0.5. In contrast, an ordinary differential equation needs to be solved numerically for the choice $r < 0.5$. Explicit finite element calculations show that most practical shock loadings can be treated as impulsive and the accuracy of the impulsive analytical predictions is confirmed. The analytical formulae are employed to determine optimal geometries of the sandwich beams that maximise the shock resistance of the beams for a given mass. The optimisation reveals that sandwich beams have a superior shock resistance relative to monolithic beams of the same mass, with the prismatic diamond core sandwich beam providing the best performance. Further, the optimal sandwich beam designs are only mildly sensitive to the length of the loading patch.

© 2005 Elsevier Ltd. All rights reserved.

Keywords: Sandwich beams; Dynamic plasticity; FE simulations; Optimal design

*Corresponding author. Tel.: +44 1223 332664; fax: +44 1223 332662.

E-mail address: vsd@eng.cam.ac.uk (V.S. Deshpande).

1. Introduction

Clamped beams are representative of many sub-structures in civilian and military vehicles. For example, the hulls of ships comprise plates welded to a linear array of primary stiffeners. Sandwich construction has potential to replace the monolithic plates conventionally employed. A major consideration in the construction of such sub-structures is their resistance to shock loading, and parallel studies by [Fleck and Deshpande \(2004\)](#) and [Xue and Hutchinson \(2004\)](#) have demonstrated the superior shock resistance of clamped sandwich beams compared to monolithic beams. While [Fleck and Deshpande \(2004\)](#) developed an analytical model for the shock resistance of clamped sandwich beams, [Xue and Hutchinson \(2004\)](#) conducted 3D dynamic Finite Element (FE) simulations to investigate the response of sandwich beams subject to impulsive loadings. In both studies, a spatially uniform transverse impulse was applied over the entire span of the beam. However, in most shock loading situations, both in practice as well as in the laboratory, beams are subjected to impulsive loading over a portion of their span.

In a recent experimental study, [Radford et al. \(2005\)](#) fired metal foam projectiles at clamped sandwich and monolithic beams of equal mass. The metal foam projectiles dynamically loaded the beams over a small patch at mid-span of the beams. In line with the theoretical predictions of [Fleck and Deshpande \(2004\)](#) and [Xue and Hutchinson \(2003\)](#); [Radford et al. \(2005\)](#) observed that for any given loading impulse, sandwich beams deflect less than monolithic beams of equal mass. This experimental investigation provides the motivation to the current study on the response of sandwich beams to impulsive loading over a central patch.

The response of clamped monolithic beams to impulsive loading over a central loading patch was first investigated by [Martin and Symmonds \(1966\)](#). They assumed small deflection theory, and they showed that the response of the monolithic beam comprises three sequential phases. The precise nature of these phases depends on whether the ratio r of the length of loading patch to beam span is greater than or less than 0.5. [Vashi \(1966\)](#) extended this analysis to account for shear deformations while more recently [Li and Jones \(1995\)](#) reported an analysis for monolithic beams loaded by a finite pressure pulse over a central loading patch.

In this study we shall determine the finite deflection response of monolithic and sandwich beams subjected to impulsive loading over a central loading patch. First, analytical formulae are presented for the finite deflection response of clamped rigid-ideally plastic monolithic and sandwich beams subjected to impulsive loads over a central patch. Next, the analytical predictions for monolithic and sandwich beams are compared with finite element simulations. Finally, the analytical formulae are used to construct performance charts for a wide range of sandwich core topologies. These performance charts are used to determine the optimal geometries of sandwich beams that maximise shock resistance for a given mass of beam.

2. Analytical model for the impulsive response of clamped monolithic beams

Consider a clamped monolithic beam of thickness H and span $2L$ subjected to an impulse I per unit beam length over a central section of length $2a$ as sketched in Fig. 1. The beam is assumed to have a uniform rectangular cross-section and is made from a rigid-ideally plastic material with yield strength σ_{fY} and material density ρ_f . The aim is to determine the finite deflection of the beam as a function of time and to characterise this by the final deflection W at mid-span of the beam and the associated structural response time T . Active plastic straining of the beam is by a combination of plastic bending and longitudinal stretching, with shear yielding neglected for the slender beams under consideration. We assume that yield of a beam element is adequately described by the resultant longitudinal force N and the bending moment M . Thus, the yield locus of the beam is given by (Jones, 1989)

$$\left(\frac{M}{M_0}\right)^2 + \frac{|N|}{N_0} = 1, \tag{1}$$

where $N_0 = \sigma_{fY}H$ and $M_0 = \sigma_{fY}H^2/4$ are the plastic values of the longitudinal force and bending moment, respectively. We approximate this yield locus to be a circumscribing square such that

$$|N| = N_0 \tag{2a}$$

$$\text{and/or } |M| = M_0, \tag{2b}$$

with yield achieved when one or both of these relations are satisfied. We could equally well approximate the yield locus to be an inscribing square such that

$$|N| = 0.618N_0 \tag{2c}$$

$$\text{and/or } |M| = 0.618M_0, \tag{2d}$$

with again at yield one or both of these relations satisfied. We proceed to develop the analysis for the circumscribing yield locus: the corresponding formulae for the inscribed locus may be obtained by replacing M_0 by $0.618M_0$ and N_0 by $0.618N_0$.

In the dynamic analysis we shall assume that displacements occur only in a direction transverse to the original axis of the beam and thus stretching is a result of only transverse displacements. Moderate transverse deflections are considered, such that the deflection w at the mid-span of the beam is assumed to be small compared to the beam length $2L$ and the longitudinal force $N = N_0$ can be assumed to be

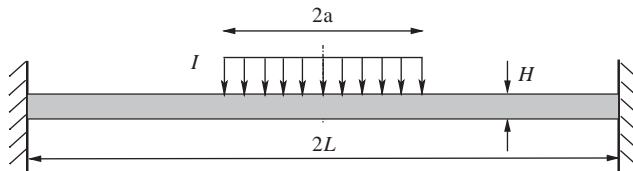


Fig. 1. Sketch of the loading geometry of the clamped monolithic beam.

constant along the beam. Following [Martin and Symmonds \(1966\)](#), the motion of the beam is then separated into three sequential phases by proposing a trial velocity distribution that satisfies the initial imposed velocity distribution (this solution can be checked, a posteriori, to confirm that the solution satisfies the yield criterion). In the first phase, the central section of the beam translates at its initial velocity $v_0 = I/(\rho_f H)$ while segments of length ξ_1 and ξ_2 rotate about plastic hinges travelling towards the supports and the mid-span, respectively, as sketched in [Fig. 2a](#). The bending moment is taken to vary from $-M_0$ at the outer plastic hinges travelling towards the supports to $+M_0$ at the hinges travelling towards the mid-span with the bending moment constant in the central flat portion. Further, since the shear force is zero at the travelling plastic hinges (bending moment is a maximum at such hinges), vertical equilibrium of the stationary outer segment of the beam dictates that the shear force at the support too is zero. Thus, time increments in curvature occur only at the ends of the rotating segments while axial straining is distributed over the length of the rotating segments. A free body diagram for half of the clamped beam is shown in [Fig. 2b](#). Conservation of linear momentum dictates that $\xi_1 = \xi_2 = \xi$ while

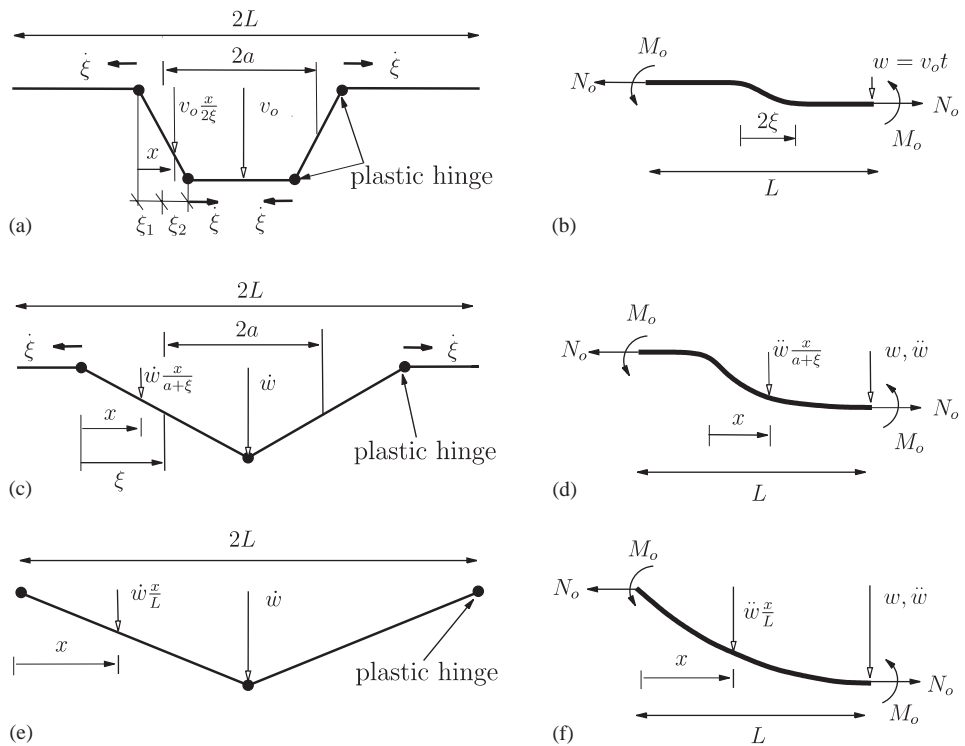


Fig. 2. Analysis of the impulsive response of a monolithic beam for $r < 0.5$, (a) Velocity profile in phase I, (b) a free body diagram of the half-beam in phase I, (c) velocity profile in phase II and (d) a free body diagram of the half-beam in phase II, (e) velocity profile in phase III and (f) a free body diagram of the half-beam in phase III.

conservation of moment of momentum about a support at time t gives

$$\begin{aligned}
 mav_0\left(L - \frac{a}{2}\right) &= m(a - \xi)v_0\left(L - \frac{a - \xi}{2}\right) \\
 &+ \int_0^{2\xi} \frac{mv_0x}{2\xi} (L - a - \xi + x) dx + 2M_0t + \frac{1}{2} N_0v_0t^2, \quad (3a)
 \end{aligned}$$

where $m = \rho_f H$ and x is an axial co-ordinate measured from the outer travelling hinge as sketched in Fig. 2a. Eq. (3a) gives ξ as a function of time via

$$\xi^2 = \frac{3t(4M_0 + N_0v_0t)}{mv_0}. \quad (3b)$$

This phase ends when the travelling plastic hinges either reach the mid-span or the supports of the beam. Depending whether $r \equiv a/L > 0.5$ or less than 0.5, the subsequent phases follow different paths. We consider each of these in turn.

2.1. Loading patch size $r < 0.5$

Phase I of the motion ends when $\xi = a$ giving the time T_1 at that instant as

$$T_1 = \frac{2M_0}{N_0v_0} \left[\sqrt{1 + \frac{N_0v_0^2ma^2}{12M_0^2}} - 1 \right], \quad (4a)$$

by substituting $\xi = a$ in Eq. (3b). The deflection of the mid-span of the beam at time T_1 is then given by

$$w_1 = T_1v_0 = \frac{2M_0}{N_0} \left[\sqrt{1 + \frac{N_0v_0^2ma^2}{12M_0^2}} - 1 \right], \quad (4b)$$

as the central portion of the beam has a constant velocity v_0 in phase I.

In phase II of the motion, a stationary plastic hinge exists at the mid-span of the beam and a pair of hinges travel towards the supports. The bending moment varies between $-M_0$ at the travelling hinges to $+M_0$ at the mid-span. The velocity profile is triangular, as sketched in Fig. 2c and the conservation of linear momentum implies that

$$mav_0 = \int_0^{a+\xi} m\dot{w} \frac{x}{a + \xi} dx, \quad (5a)$$

where \dot{w} is the velocity at the mid-span and x an axial co-ordinate measured from the current position of the travelling hinge towards the mid-span. Thus, equation simplifies to give the relation between the velocity \dot{w} and the travelling hinge position ξ as

$$\frac{v_0}{\dot{w}} = \frac{1}{2} + \frac{\xi}{2a}. \quad (5b)$$

Conservation of moment of momentum about one of the supports at time t gives

$$mav_0\left(L - \frac{a}{2}\right) = \int_0^{a+\xi} \frac{m\dot{w}x}{a+\xi} (L - a - \xi + x)dx + 2M_0t + N_0 \int_0^t w(t) dt. \tag{6}$$

We obtain the governing differential equation for this phase by substituting for \dot{w} in Eq. (6) from Eq. (5b) and differentiating twice with respect to time, to give

$$\frac{1}{6}m(a + \xi)\ddot{\xi} = N_0, \tag{7}$$

where the over-dot denotes differentiation with respect to time. The solution of this ODE with initial conditions

$$\xi(T_1) = a, \quad \text{and} \tag{8a}$$

$$\dot{\xi}(T_1) = \frac{1}{mav_0} (6M_0 + 3N_0w_1), \tag{8b}$$

gives the position of the travelling hinge as a function of time in phase II of the motion. The initial condition (8b) is obtained by differentiating Eq. (6) once with respect to time t and substituting $t = T_1$ and $w(T_1) = w_1$. This phase ends at time T_2 when the travelling hinges reach the support, i.e. at a time when $\xi = L - a$. Thus, the displacement w_2 in this phase is obtained from Eq. (5b) as

$$w_2 = \int_{T_1}^{T_2} \frac{2v_0a}{a + \xi(t)} dt. \tag{9}$$

Note that the velocity at the mid-span $\dot{w} = 2rv_0$ at time T_2 .

In phase III of the motion, stationary plastic hinges exist at the mid-span and at the ends of the beam, with the moment varying between $-M_0$ at the beam end to $+M_0$ at the mid-span. The velocity profile is triangular, as sketched in Fig. 2e. The equation of motion of the half-beam in phase III follows from the free-body diagram sketched in Fig. 2f as

$$2M_0 + N_0w = -\frac{\ddot{w}}{L} \int_0^L mx^2 dx = -\frac{mL^3}{3} \frac{\ddot{w}}{L}, \tag{10}$$

where x is the axial co-ordinate from one end of the beam as shown in Fig. 2f. With initial conditions $w(T_2) = w_1 + w_2$ and $\dot{w}(T_2) = 2rv_0$, this differential equation admits a solution of the form

$$w(t) = \frac{\dot{w}(T_2)}{\omega} \sin[\omega(t - T_2)] + \left(\frac{2M_0}{N_0} + w_1 + w_2\right) \cos[\omega(t - T_2)] - \frac{2M_0}{N_0}, \tag{11a}$$

where

$$\omega = \frac{1}{L} \sqrt{\frac{3N_0}{m}}. \tag{11b}$$

The maximum deflection W of the mid-span of the beam occurs at a time T when $\dot{w}(T) = 0$. Upon substituting this termination condition in the velocity equation, as

given by the time derivative of Eq. (11a), the response time T is obtained as

$$T = T_2 + \frac{1}{\omega} \tan^{-1} \left[\frac{2rN_0v_0}{\omega(2M_0 + (w_1 + w_2)N_0)} \right], \tag{12}$$

and the corresponding maximum deflection of the mid-span of the beam is

$$W = \sqrt{\frac{\dot{w}(T_2)^2}{\omega^2} + \left(\frac{2M_0}{N_0} + w_1 + w_2 \right)^2} - \frac{2M_0}{N_0}. \tag{13}$$

We proceed to present these equations in non-dimensional form by introducing the non-dimensional variables

$$\bar{I} \equiv \frac{I}{L\sqrt{\sigma_{fY}\rho_f}} = \frac{mv_0}{L\sqrt{\sigma_{fY}\rho_f}}, \tag{14a}$$

$$\bar{T} \equiv \frac{T}{L\sqrt{\rho_f/\sigma_{fY}}}, \tag{14b}$$

$$\bar{W} \equiv \frac{W}{L}, \quad \text{and} \tag{14c}$$

$$\bar{H} \equiv \frac{H}{L}. \tag{14d}$$

The mid-span deflection and time period of phase I of the motion are given in non-dimensional form by

$$\bar{w}_1 = \frac{w_1}{L} = \frac{\bar{H}}{2} \left[\sqrt{1 + \frac{4}{3} \frac{r^2 \bar{I}^2}{\bar{H}^4}} - 1 \right], \quad \text{and} \tag{15a}$$

$$\bar{T}_1 = \frac{T_1}{L\sqrt{\rho_f/\sigma_{fY}}} = \frac{\bar{H}^2}{2\bar{I}} \left[\sqrt{1 + \frac{4}{3} \frac{r^2 \bar{I}^2}{\bar{H}^4}} - 1 \right], \tag{15b}$$

respectively, while the governing differential for phase II of the motion is

$$(r + \bar{\xi})\ddot{\bar{\xi}} = 6, \tag{16}$$

with initial conditions

$$\bar{\xi}(\bar{T}_1) = r, \quad \text{and} \tag{17a}$$

$$\dot{\bar{\xi}}(\bar{T}_1) = \frac{3\bar{H}}{2r\bar{I}} (\bar{H} + 2\bar{w}_1), \tag{17b}$$

where $\bar{\xi} \equiv \xi/L$. This phase ends when $\bar{\xi}(\bar{T}_2) = 1 - r$ and the deflection of the mid-span in phase II is given by

$$\bar{w}_2 = \frac{w_2}{L} = \int_{\bar{T}_1}^{\bar{T}_2} \dot{w} \, d\bar{t} \tag{18a}$$

where the normalised velocity \dot{w} of the mid-span is given by

$$\dot{w} = \dot{w} \sqrt{\rho_f / \sigma_{fY}} = \frac{2r\bar{I}}{\bar{H}(r + \bar{\xi})}. \tag{18b}$$

Employing the phase III analysis detailed above, the non-dimensional maximum deflection of the mid-span and structural response time are given by

$$\bar{W} = \frac{\bar{H}}{2} \left[\sqrt{\left(1 + \frac{2(\bar{w}_1 + \bar{w}_2)}{\bar{H}}\right)^2 + \frac{16}{3} \frac{r^2 \bar{I}^2}{\bar{H}^4}} - 1 \right], \tag{19a}$$

and

$$\bar{T} = \bar{T}_2 + \frac{1}{\sqrt{3}} \tan^{-1} \left(\frac{4}{\sqrt{3}} \frac{r\bar{I}}{\bar{H}[\bar{H} + 2(\bar{w}_1 + \bar{w}_2)]} \right), \tag{19b}$$

respectively.

An approximate closed-form solution giving the maximum deflection of the mid-span and the structural response time is presented in Appendix A. In this solution we neglect the deflections in phases I and II and consider only the deflection in the “modal solution” corresponding to phase III. As will be seen subsequently, this approximate solution under-predicts the deflection but may suffice for initial design purposes.

2.2. Loading patch size $r > 0.5$

For $r > 0.5$ phase I ends when the travelling hinges reach the outer supports, i.e. when $\xi = L - a$. Substituting this condition in Eq. (3b) gives the time period of this phase as

$$T_1 = \frac{H}{2v_0} \left[\sqrt{1 + \frac{(1-r)^2}{3} \frac{mv_0^2 L^2}{M_0 H}} - 1 \right], \tag{20a}$$

and the mid-span deflection at the end of phase I is given by

$$w_1 = v_0 T_1 = \frac{H}{2} \left[\sqrt{1 + \frac{(1-r)^2}{3} \frac{mv_0^2 L^2}{M_0 H}} - 1 \right]. \tag{20b}$$

In phase II, the central portion of the beam continues to translate at the initial velocity v_0 while adjacent segments of length ξ' rotate about the supports as sketched in Fig. 3c. The bending moment is taken to vary from $-M_0$ at the outer stationary plastic hinges at the supports to $+M_0$ at the ends of the segments of length ξ' , with

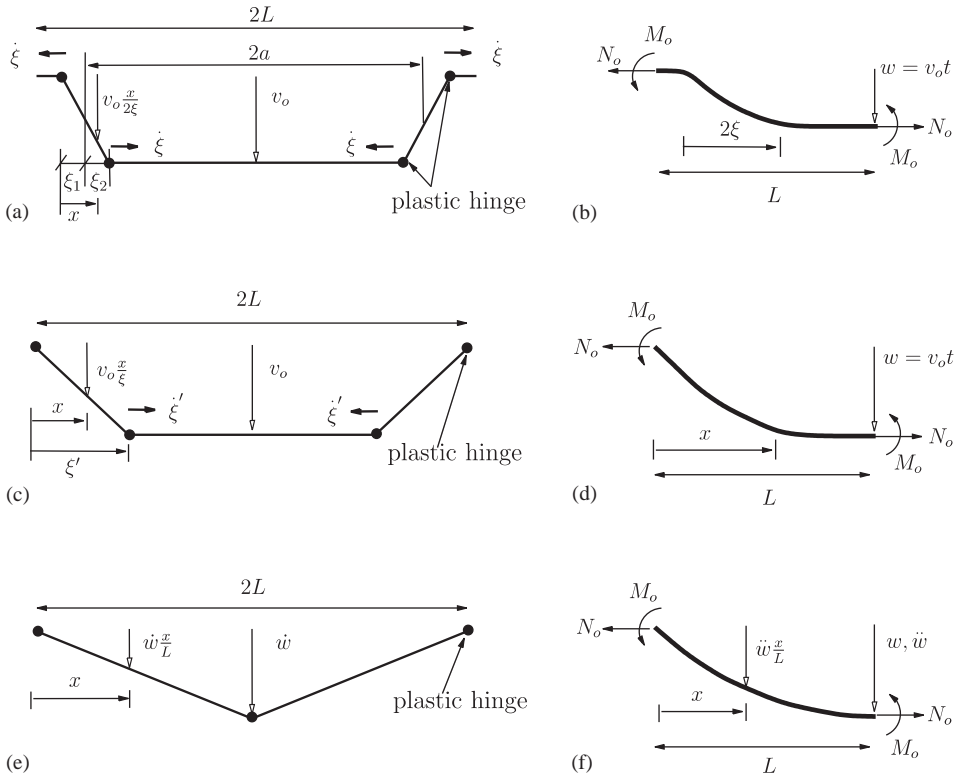


Fig. 3. Analysis of the impulsive response of a monolithic beam for $r > 0.5$, (a) Velocity profile in phase I, (b) a free body diagram of the half-beam in phase I, (c) velocity profile in phase II and (d) a free body diagram of the half-beam in phase II, (e) velocity profile in phase III and (f) a free body diagram of the half-beam in phase III.

the bending moment constant in the central flat portion. Thus, time increments in curvature occur only at the ends of the rotating segments while axial straining is distributed over the length of the rotating segments. A free body diagram for half of the clamped beam is shown in Fig. 3d; conservation of the moment of momentum about a fixed end after a time t gives

$$\begin{aligned}
 mav_0 \left(L - \frac{a}{2} \right) &= m(L - \xi')v_0 \left(\xi' + \frac{L - \xi'}{2} \right) + 2M_0t \\
 &+ \frac{1}{2} N_0v_0t^2 + \int_0^{\xi'} \frac{mv_0x^2}{\xi'} dx,
 \end{aligned}
 \tag{21}$$

which simplifies to give

$$\xi'^2 = 3L^2(1 - r)^2 + \frac{3t(N_0v_0t + 4M_0)}{mv_0}.
 \tag{22}$$

This phase ends when $\xi' = L$ and thus the accumulated T_2 at the end this phase and the total displacement $w_1 + w_2$ of the mid-span at time T_2 are given by

$$T_2 = \frac{H}{2v_0} \left[\sqrt{1 - \left(r^2 - 2r + \frac{2}{3}\right) \frac{mv_0^2 L^2}{M_0 H}} - 1 \right], \tag{23a}$$

and

$$w_1 + w_2 = v_0 T_2 = \frac{H}{2} \left[\sqrt{1 - \left(r^2 - 2r + \frac{2}{3}\right) \frac{mv_0^2 L^2}{M_0 H}} - 1 \right], \tag{23b}$$

respectively.

Phase III of the motion resembles that for the beam of $r < 0.5$. Stationary plastic hinges exist at mid-span and at the ends of the beam similar, and the equation of motion is given by Eq. (10) with initial conditions $w(T_2) = w_1 + w_2$ as specified by Eq. (23b) and $\dot{w}(T_2) = v_0$. The overall structural response time T and the associated maximum deflection at mid-span follow as:

$$T = T_2 + \frac{1}{\omega} \tan^{-1} \left[\frac{N_0 v_0}{\omega(2M_0 + (w_1 + w_2)N_0)} \right] \tag{24a}$$

and

$$W = \sqrt{\frac{v_0^2}{\omega^2} + \left(\frac{2M_0}{N_0} + w_1 + w_2\right)^2} - \frac{2M_0}{N_0}, \tag{24b}$$

respectively. There expressions can be re-written in non-dimensional form as

$$\begin{aligned} \bar{T} = \frac{\bar{H}^2}{2\bar{I}} & \left[\sqrt{1 - 4\left(r^2 - 2r + \frac{2}{3}\right) \frac{\bar{I}^2}{\bar{H}^4}} - 1 \right] \\ & + \frac{1}{\sqrt{3}} \tan^{-1} \left(\frac{2}{\sqrt{3}} \frac{\bar{I}}{\bar{H}^2} \frac{1}{[1 - 4(r^2 - 2r + 2/3)\bar{I}^2/\bar{H}^4]^{1/2}} \right), \end{aligned} \tag{25a}$$

and

$$\bar{W} = \frac{\bar{H}}{2} \left[\sqrt{1 - 4\left(r^2 - 2r + \frac{1}{3}\right) \frac{\bar{I}^2}{\bar{H}^4}} - 1 \right], \tag{25b}$$

respectively. The above derivation reduces to that of [Fleck and Deshpande \(2004\)](#) in the limit $r = 1$. It is worth emphasising here that all the results presented above (for both $r < 0.5$ and $r > 0.5$) employ the circumscribing yield locus. These results can be readily transformed to those for the inscribing yield locus by replacing σ_{fY} by $0.618\sigma_{fY}$. Explicit formulae for the inscribing yield locus are omitted here for the sake of brevity.

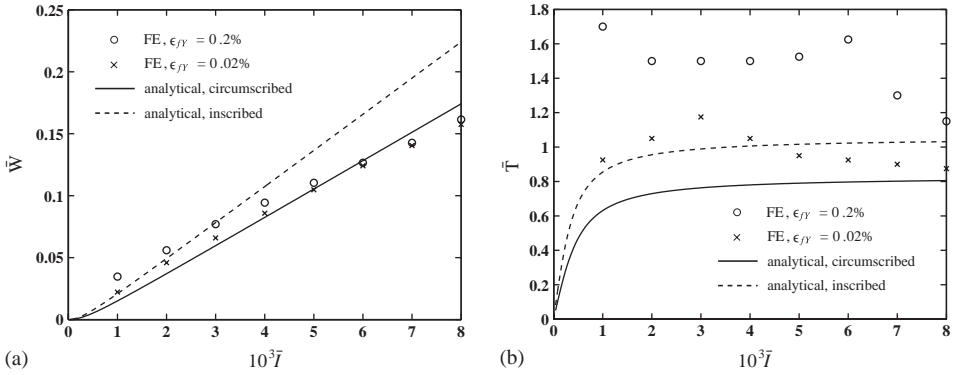


Fig. 4. Response of a clamped monolithic beam ($\bar{H} = 0.02$) with loading patch size $r = 0.3$. (a) The normalised deflection \bar{W} and (b) the structural response time \bar{T} are plotted as a function of the impulse \bar{I} . Analytical predictions employing the inscribing and circumscribing yield locus along with FE predictions for two choices of the material yield strain ϵ_{fY} are included.

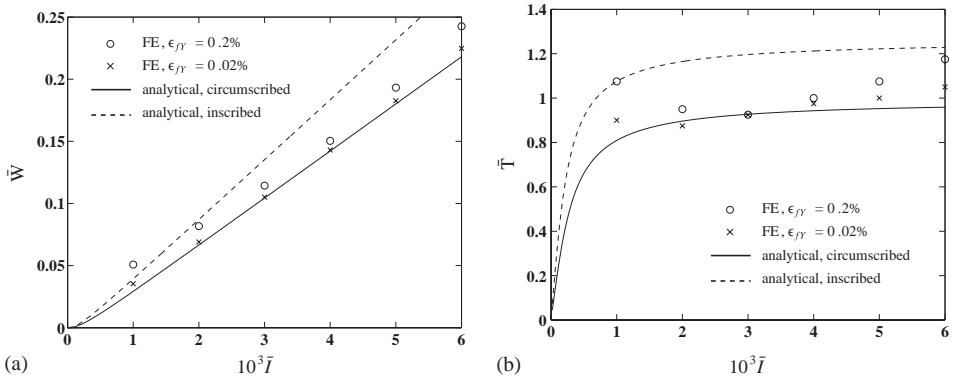


Fig. 5. Response of a clamped monolithic beam ($\bar{H} = 0.02$) with loading patch size $r = 0.7$. (a) The normalised deflection \bar{W} and (b) the structural response time \bar{T} are plotted as a function of the impulse \bar{I} . Analytical predictions employing the inscribing and circumscribing yield locus along with FE predictions for two choices of the material yield strain ϵ_{fY} are included.

2.3. Predictions of the model

We proceed to illustrate graphically the predictions of the model. Consider a monolithic beam with slenderness ratio $\bar{H} = 0.02$ made from a rigid ideally-plastic material. The maximum normalised deflection \bar{W} at mid-span of the beam and the structural response time \bar{T} are plotted in Figs. 4a and b as a function of the normalised impulse for an impulse applied over a central patch of size $r = 0.3$ and in Fig. 5 for $r = 0.7$. Predictions employing both the inscribing and circumscribing yield

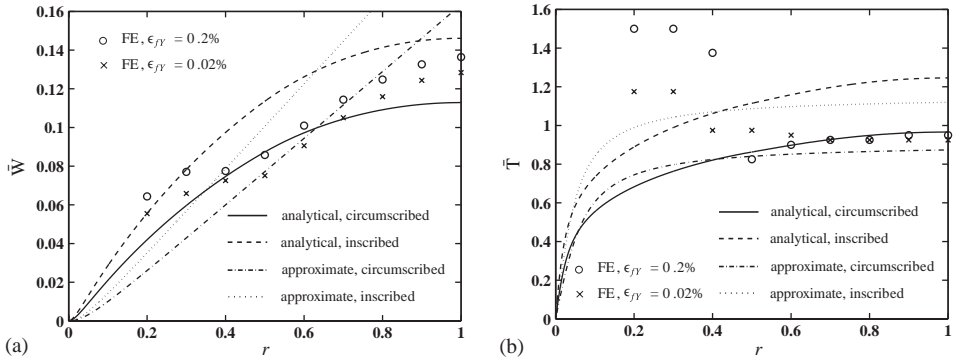


Fig. 6. Response of a clamped monolithic beam ($\bar{H} = 0.02$) subject to a normalised impulse per unit area $\bar{I} = 0.003$. (a) The normalised deflection \bar{W} and (b) the structural response time \bar{T} are plotted as a function of the loading patch size r . Analytical predictions employing the inscribing and circumscribing yield locus along with FE predictions for two choices of the material yield strain ϵ_{fy} are included.

loci are included. Over the range of impulses considered, \bar{W} increases approximately linearly with \bar{I} . \bar{T} also increases linearly with \bar{I} at small \bar{I} , but at high impulses the beam behaves as a stretched plastic string and \bar{T} becomes almost independent of the magnitude of \bar{I} .

We now consider the effect of the loading patch size by considering two cases in turn. First consider the case of a fixed impulse per unit area. The maximum normalised mid-span deflection \bar{W} and structural response time \bar{T} are plotted in Figs. 6a and b, respectively, as a function of the loading patch size r for a fixed normalised impulse per unit area $\bar{I} = 0.003$. Predictions employing both the inscribing and circumscribing yield loci are included along with predictions of the approximate modal analysis. While the approximate analysis predicts the structural response time with reasonable accuracy it is not accurate for estimating the maximum deflections. Second, consider the case of a fixed total impulse. The maximum deflection \bar{W} and structural response time \bar{T} for a fixed normalised total impulse $\bar{I}r = 0.003$ are plotted in Figs. 7a and b, respectively. Again, predictions employing both the inscribing and circumscribing yield loci are plotted along with the approximate predictions. The full analysis predicts that as the loading patch size r is decreased, the deflections increase while the response time decreases. On the other hand, the approximate analysis predicts that the deflections and response time depend only on the total impulse $\bar{I}r$ and are independent of r in Fig. 7a.

3. Analytical model for the impulsive response of clamped sandwich beams

Fleck and Deshpande (2004) analysed the impulsive response of clamped sandwich beams subject to an impulse applied over the entire span of the beam. This model is now extended to analyse the response of clamped sandwich beams

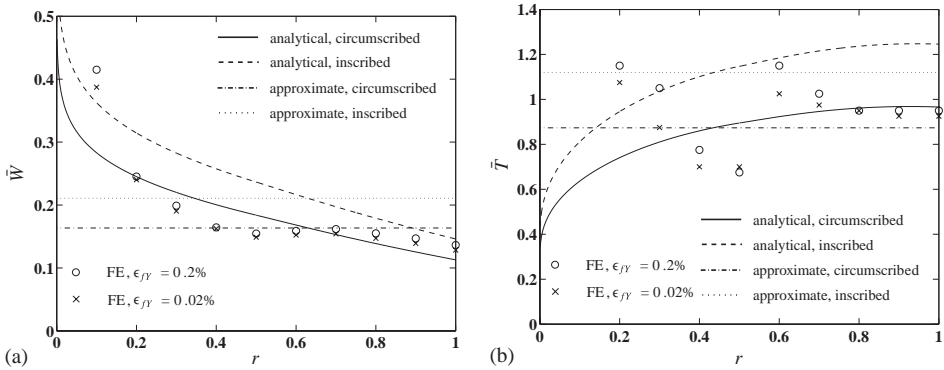


Fig. 7. Response of a clamped monolithic beam ($\bar{H} = 0.02$) subject to a total normalised impulse $\bar{I}r = 0.003$. (a) The normalised deflection \bar{W} and (b) the structural response time \bar{T} are plotted as a function of the loading patch size r . Analytical predictions employing the inscribing and circumscribing yield locus along with FE predictions for two choices of the material yield strain ϵ_{fY} are included.

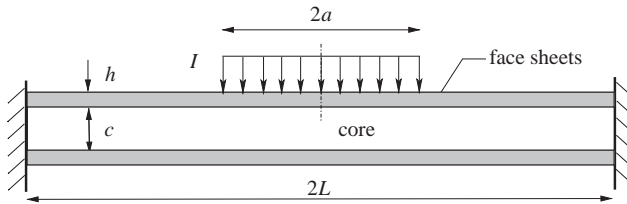


Fig. 8. Sketch of the loading geometry of the clamped sandwich beam.

subject to a spatially uniform impulse over a central patch of the beam as sketched in Fig. 8.

Consider a clamped sandwich beam of span $2L$ with identical face-sheets of thickness h and a core of thickness c , see Fig. 8. The face-sheets are made from a rigid ideally-plastic solid of yield strength σ_{fY} , density ρ_f . The core is taken to be a compressible solid of density ρ_c . In line with the measured stress versus strain responses of cellular materials like metal foams, it is assumed that the core compresses at a constant stress σ_n in a direction transverse to the beam length with no lateral expansion up to a densification strain ϵ_D ; beyond densification the core is treated as rigid. The axial or longitudinal tensile strength of the core is taken to be σ_1 . Similar to Fleck and Deshpande (2004) we split the response of the sandwich structure into three sequential stages:

- (i) Stage I—fluid–structure interaction phase, which is neglected here and the entire impulse I of the shock is transmitted to the front face of the sandwich beam over a central patch of length $2a$. This assumption is valid for a shock wave in air as discussed in Fleck and Deshpande (2004).

- (ii) Stage II—core compression phase, and
- (iii) Stage III—beam bending and stretching phase.

The justification for splitting the analysis into three distinct stages is the observation by Fleck and Deshpande (2004) that the time-periods for the three phases differ significantly. We develop a model by employing this assumption and subsequently justify the separation into stages II and III (recall that the fluid–structure interaction phase is neglected in this analysis) it via detailed FE simulations.

3.1. Stage II—core compression phase

At the start of this phase, the front face has a velocity $v_0 = I/(\rho_f h)$ over a central patch of length $2a$ while the rest of the beam is stationary. We assume that in the subsequent core compression phase there is momentum transfer from the front face to the core and rear face immediately below the loading patch but no momentum is transferred to any other portion of the beam. Thus, any bending effects are neglected and this phase reduces to the 1D core compression problem as analysed by Fleck and Deshpande (2004). Upon employing the assumption that there is no momentum transferred to and from the central portion of length $2a$ of the beam, momentum conservation dictates that the final common velocity v of the sandwich beam cross-section over the central patch of length $2a$ is given by

$$v = \frac{I}{2\rho_f h + \rho_c c}. \quad (26)$$

Thus, the ratio of the energy lost in this phase U_{lost} to the initial kinetic energy $I^2/2\rho_f h$ of the front face is given by

$$\phi \equiv \frac{U_{\text{lost}}}{I^2/(2\rho_f h)} = \frac{1+q}{2+q}, \quad (27)$$

where $q = \rho_c c/(\rho_f h)$ is the ratio of the mass of the core to the mass of a face sheet. This energy lost is dissipated by plastic dissipation in compressing the core at a stress σ_n resulting in an average through-thickness core compression strain ε_c

$$\varepsilon_c = \frac{\bar{I}^2}{2\bar{\sigma}_n \bar{c}^2 \bar{h}} \frac{\bar{h} + \bar{\rho}}{2\bar{h} + \bar{\rho}}, \quad (28)$$

where $\bar{h} \equiv h/c$, $\bar{c} \equiv c/L$, $\bar{\rho} \equiv \rho_c/\rho_f$, $\bar{I} \equiv I/(L\sqrt{\sigma_{fY}\rho_f})$ and $\bar{\sigma}_n \equiv \sigma_n/\sigma_{fY}$. However, if U_{lost} is too high such that ε_c as given by Eq. (28) exceeds the densification strain ε_D , then ε_c is set equal to ε_D and the analysis does not explicitly account for the additional dissipation mechanisms required to conserve energy. Rather it is assumed that inelastic impact of the front face against the combined core and rear face leads to the additional dissipation. After the core has compressed by a strain of ε_c , the core height is reduced to $c' = (1 - \varepsilon_c)c$.

Fleck and Deshpande (2004) have estimated the time taken for the front and rear faces to attain a common velocity by analysing a plastic shock wave propagating

through the core. An approximate closed-form expression for the core compression time T_c is obtained by neglecting the core mass, and is given by

$$\bar{T}_c \equiv \frac{T_c}{L\sqrt{\rho_f/\sigma_{fY}}} = \begin{cases} \frac{\bar{I}}{2\bar{\sigma}_n} & \text{if } \bar{I}^2 < 4\bar{\sigma}_n c^2 \bar{h}\epsilon_D, \\ \frac{\bar{I}}{2\bar{\sigma}_n} \left[1 - \sqrt{1 - \frac{4\bar{\sigma}_n c^2 \bar{h}\epsilon_D}{\bar{I}^2}} \right] & \text{otherwise.} \end{cases} \quad (29)$$

As mentioned above, T_c is small compared to the structural response time of the sandwich beam and thus following Fleck and Deshpande (2004), we neglect the transverse deflection of the rear face of the sandwich beam in this stage.

3.2. Stage III—beam bending and stretching phase

At the end of stage II, the cross-section of the sandwich beam over a central patch of length $2a$ has a core thickness $c' = c(1 - \epsilon_c)$ and a velocity v . The remaining portion of the beam (with core thickness c) is stationary. Thus, the problem is reduced to the monolithic beam problem analysed previously, albeit the sandwich beam has a non-uniform cross-sectional thickness.

The shape of the yield surface of a sandwich beam in (N, M) space depends upon the relative strength and thickness of the faces and the core. The yield locus

$$\frac{|M|}{M_0} + \frac{|N|}{N_0} = 1, \quad (30)$$

where N_0 and M_0 are the plastic collapse values of the longitudinal force and bending moment, respectively, is highly accurate for a sandwich beam with thin, strong faces and a thick, weak core. It becomes less accurate as the beam section approaches the monolithic limit. Similar to the monolithic beam case, we approximate this yield locus by either a circumscribing or inscribing square such that

$$|N| = N_0 \quad (31a)$$

$$\text{and/or } |M| = M_0, \quad (31b)$$

and

$$|N| = 0.5N_0 \quad (32a)$$

$$\text{and/or } |M| = 0.5M_0, \quad (32b)$$

respectively.

The longitudinal plastic membrane force N_0 is assumed to be insensitive to the degree of core compression and is thus given by

$$N_0 = 2h\sigma_{fY} + \sigma_1 c, \quad (33)$$

over the entire beam length. However, the plastic bending moment of the beam is reduced by core compression. The plastic bending moment over the uncompressed

section M_{ou} , and over the compressed section M_{oc} are given by

$$M_{ou} = \sigma_{fY} \frac{(c + 2h)^2}{4} - \sigma_{fY} \frac{c^2}{4} + \sigma_1 \frac{c^2}{4}, \tag{34a}$$

and

$$M_{oc} = \sigma_{fY} \frac{(c' + 2h)^2}{4} - \sigma_{fY} \frac{c'^2}{4} + \frac{\sigma_1}{(1 - \epsilon_c)} \frac{c'^2}{4}, \tag{34b}$$

respectively. Note that the $\sigma_1/(1 - \epsilon_c)$ term in Eq. (34b) arises from the fact that we have assumed that the plastic membrane force of the core is insensitive to core compression.

The analysis for the monolithic beams presented in Section 2 can be readily extended to sandwich beams by noting that the plastic bending moment of the hinges travelling towards the mid-span equals M_{oc} while that of the hinges travelling towards the supports is M_{ou} . Further, N_0 is identified as the longitudinal strength of the sandwich beam and given by Eq. (33) while the mass per unit length of the sandwich beam is given by

$$m = 2\rho_f h + \rho_c c. \tag{35}$$

The detailed analysis is omitted here for the sake of brevity and we proceed to give the formulae for the maximum deflection structural response time of the sandwich beams in non-dimensional form.

The non-dimensional geometric variables of the sandwich beam are

$$\bar{c} \equiv \frac{c}{L}, \quad \bar{h} \equiv \frac{h}{c}, \quad \hat{c} \equiv \bar{c}(1 - \epsilon_c), \quad \text{and}, \quad \hat{h} \equiv \frac{\bar{h}}{1 - \epsilon_c}, \tag{36}$$

while the non-dimensional core properties are given by

$$\bar{\rho} \equiv \frac{\rho_c}{\rho_f}, \quad \bar{\sigma}_1 \equiv \frac{\sigma_1}{\sigma_{fY}}, \quad \bar{\sigma}_n \equiv \frac{\sigma_n}{\sigma_{fY}} \quad \text{and} \quad \hat{\sigma}_1 \equiv \frac{\bar{\sigma}_1}{1 - \epsilon_c}. \tag{37}$$

The non-dimensional structural response time \bar{T} and shock impulse \bar{I} are

$$\bar{T} \equiv \frac{T}{L} \sqrt{\frac{\sigma_{fY}}{\rho_f}} \quad \text{and} \quad \bar{I} \equiv \frac{I}{L\sqrt{\rho_f\sigma_{fY}}}, \tag{38}$$

respectively. The formulae for the deflection and structural response time are presented below in terms of the parameters

$$\alpha_1 = \bar{c}^2[(1 + 2\bar{h})^2 - 1 + \bar{\sigma}_1] + \hat{c}^2[(1 + 2\hat{h})^2 - 1 + \hat{\sigma}_1], \tag{39a}$$

$$\alpha_2 = \sqrt{\frac{2\bar{h} + \bar{\sigma}_1}{2\bar{h} + \bar{\rho}}}, \quad \text{and} \tag{39b}$$

$$\alpha_3 = \frac{1}{4\bar{c}(2\bar{h} + \bar{\sigma}_1)}. \tag{39c}$$

All the formulae presented below are for the choice of a circumscribing yield locus. Predictions for the inscribing yield locus can be easily obtained by replacing σ_{fY} by $0.5\sigma_{fY}$ in the definitions of \bar{I} and \bar{T} .

3.3. Loading patch size $r < 0.5$

The normalised structural response time, and the maximum deflection at mid-span of the rear face sheet of the sandwich beam, are given by

$$\bar{T} = \bar{T}_2 + \frac{1}{\sqrt{3}\alpha_2} \tan^{-1} \left(\frac{8}{\sqrt{3}} \frac{\alpha_2\alpha_3}{\alpha_1\alpha_3 + \bar{w}_1 + \bar{w}_2} \bar{I}r \right), \tag{40a}$$

and

$$\bar{W} \equiv \frac{W}{L} = (\alpha_1\alpha_3 + \bar{w}_1 + \bar{w}_2) \sqrt{1 + \frac{64}{3} \frac{\alpha_2^2\alpha_3^2}{(\alpha_1\alpha_3 + \bar{w}_1 + \bar{w}_2)^2} \bar{I}^2 r^2 - \alpha_1\alpha_3}, \tag{40b}$$

respectively. The non-dimensional deflection \bar{w}_1 and time \bar{T}_1 at the end of phase I of the motion ends are given by

$$\bar{w}_1 = \alpha_1\alpha_3 \left(\sqrt{1 + \frac{16}{3} \frac{\alpha_2^2}{\alpha_1^2} \bar{I}^2 r^2} - 1 \right), \tag{41a}$$

and

$$\bar{T}_1 = \frac{1}{4\bar{I}} \frac{\alpha_1}{\alpha_2^2} \left(\sqrt{1 + \frac{16}{3} \frac{\alpha_2^2}{\alpha_1^2} \bar{I}^2 r^2} - 1 \right), \tag{41b}$$

respectively. No closed-form expressions exist for the deflection \bar{w}_2 during phase II of the motion and the time \bar{T}_2 at which phase II ends. These can be obtained numerically as follows. The deflection \bar{w}_2 is given by

$$\bar{w}_2 = \int_{\bar{T}_1}^{\bar{T}_2} \frac{8\alpha_2^2\alpha_3\bar{I}r}{r + \bar{\xi}(\bar{t})} d\bar{t}, \tag{42}$$

where $\bar{\xi}(\bar{t})$ is the differential equation

$$(r + \bar{\xi})\ddot{\bar{\xi}}(\bar{t}) = 6\alpha_2^2, \tag{43a}$$

with initial conditions

$$\bar{\xi}(\bar{T}_1) = r, \quad \text{and} \quad \dot{\bar{\xi}}(\bar{T}_1) = \frac{3}{4\bar{I}r} \left(\alpha_1 + \frac{\bar{w}_1}{\alpha_3} \right). \tag{43b}$$

The termination condition for phase II of the motion, gives the time \bar{T}_2 as

$$\bar{\xi}(\bar{T}_2) = 1 - r. \tag{43c}$$

The deflection w_0 at the mid-span of the front face sheet is given by

$$\bar{w}_0 \equiv \frac{w_0}{L} = \bar{W} + \bar{c}\epsilon_c. \tag{44}$$

3.4. Loading patch size $r > 0.5$

Closed-form expressions for \bar{W} and \bar{T} exist for $r > 0.5$ and are given by

$$\bar{W} = \alpha_1 \alpha_3 \left(\sqrt{1 + \frac{16}{3} \frac{\alpha_2^2}{\alpha_1^2} (-3r^2 + 6r - 1) \bar{I}^2} - 1 \right) \tag{45a}$$

and

$$\bar{T} = \frac{1}{4\bar{I}\alpha_2^2} \left(\sqrt{\alpha_1^2 + \frac{16}{3} \alpha_2^2 (-3r^2 + 6r - 2) \bar{I}^2} - \alpha_1 \right) + \frac{1}{\alpha_2 \sqrt{3}} \tan^{-1} \left(\frac{4\alpha_2 \bar{I}}{\sqrt{3\alpha_1^2 + 16\alpha_2^2 (-3r^2 + 6r - 2) \bar{I}^2}} \right), \tag{45b}$$

respectively.

3.5. Predictions of the model

We proceed to graphically illustrate the predictions of the model. All results are presented for a representative sandwich beam with $\bar{c} = 0.03$, $\bar{h} = 0.1$ and comprising an isotropic core of relative density $\bar{\rho} = 0.1$ made from the same solid material as the face sheets. The non-dimensional strengths of the core are taken to be $\bar{\sigma}_n = \bar{\sigma}_l = 0.5\bar{\rho} = 0.05$ which is representative of an octet truss lattice material (Deshpande et al., 2001), while the densification strain of the core is assumed to be $\epsilon_D = 0.5$.

The maximum normalised deflection \bar{W} of the rear face of the sandwich beam and core compression ϵ_c are plotted in Fig. 9a as a function of the normalised impulse for

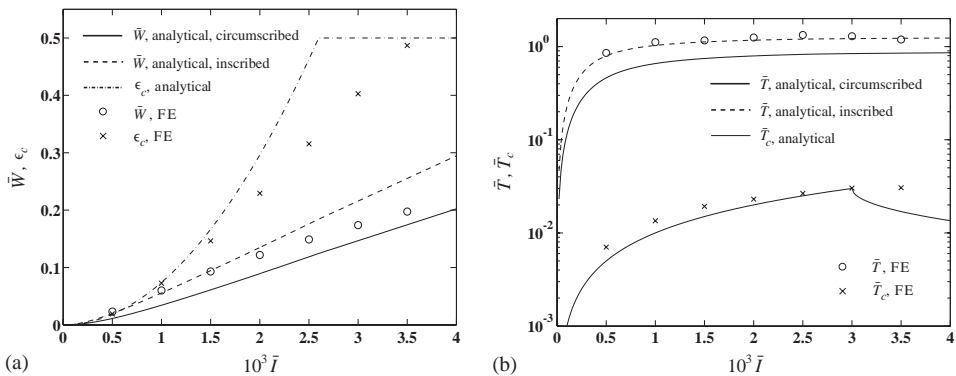


Fig. 9. Response of a clamped sandwich beam ($\bar{c} = 0.03$, $\bar{h} = 0.1$) with an isotropic core ($\bar{\rho} = 0.1$, $\bar{\sigma}_n = \bar{\sigma}_l = 0.05$, $\epsilon_D = 0.5$) with $r = 0.3$. (a) The normalised deflection \bar{W} and core compression ϵ_c (b) structural response time \bar{T} and core compression time \bar{T}_c , as a function of the normalised impulse \bar{I} . Analytical predictions employing the inscribing and circumscribing yield locus (for \bar{W} and \bar{T}) are included along with FE predictions.

an impulse applied over a central patch of size $r = 0.3$. Predictions of \bar{W} employing both the inscribing and circumscribing yield loci are included (recall that the core compression is independent of the choice of the yield locus). For $\bar{I} < 0.0025$, the compressive strain ε_c induced in the core in Stage II is less than ε_D and \bar{W} increases approximately quadratically with \bar{I} . At higher impulses the core compression is fixed at the densification limit ε_D and \bar{W} increases almost linearly with \bar{I} . The structural response time \bar{T} (employing both the inscribing and circumscribing yield loci) and the estimate for the core compression time \bar{T}_c (29) are plotted in Fig. 9b, as a function of the impulse \bar{I} . The structural response time initially increases approximately linearly with \bar{I} , but at high impulses the beam behaves like a stretched plastic string and \bar{T} is almost independent of the magnitude of \bar{I} . On the other hand, the core compression time increases with \bar{I} up to $\bar{I} \approx 0.003$: for higher impulses the core is fully densified and the core compression time reduces with increasing impulse. Importantly, we see that the core compression time is about two orders of magnitude smaller than the structural response time, in support of the decoupling of the two stages assumed in the analysis.

We now consider the effect of the loading patch size by considering the two cases of a fixed impulse per unit area and a fixed total impulse, in turn. First consider the case of a fixed impulse per unit area $\bar{I} = 0.002$. The predictions for \bar{W} employing the inscribing and circumscribing yield loci are plotted in Fig. 10a as a function of the patch size r . Similarly the predictions of \bar{T} and \bar{T}_c are plotted in Fig. 10b: \bar{T}_c is independent of r while for this level of impulse, the structural response time \bar{T} is also approximately constant for $r > 0.2$.

Predictions for a fixed total impulse $\bar{I}r = 0.002$ are plotted in Figs. 11a and b. Similar to the monolithic beam case, \bar{W} increases with decreasing r while \bar{T} is relatively insensitive to r . The core compression time \bar{T}_c is maximum at $r \approx 0.7$: for larger values of r the core compression strain ε_c does not attain the densification

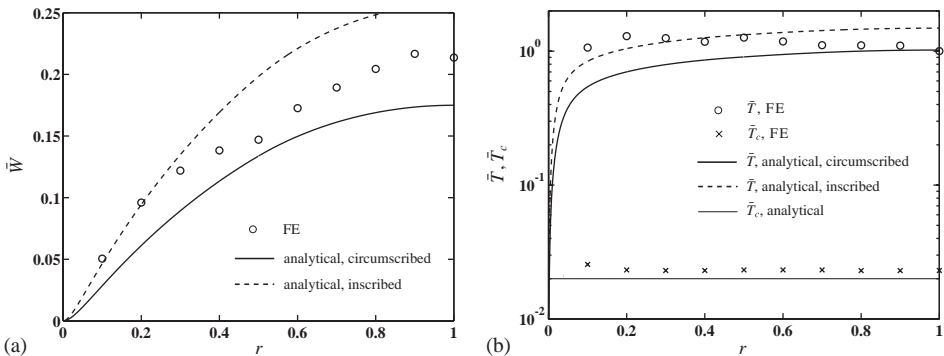


Fig. 10. Response of a clamped sandwich beam ($\bar{c} = 0.03$, $\bar{h} = 0.1$) with an isotropic core ($\bar{\rho} = 0.1$, $\bar{\sigma}_n = \bar{\sigma}_t = 0.05$, $\varepsilon_D = 0.5$) subject to an impulse per unit area $\bar{I} = 0.002$. (a) The normalised deflection \bar{W} and (b) structural response time \bar{T} and core compression time \bar{T}_c , as a function of patch loading size r . Analytical predictions employing the inscribing and circumscribing yield locus (for \bar{W} and \bar{T}) are included along with FE predictions.

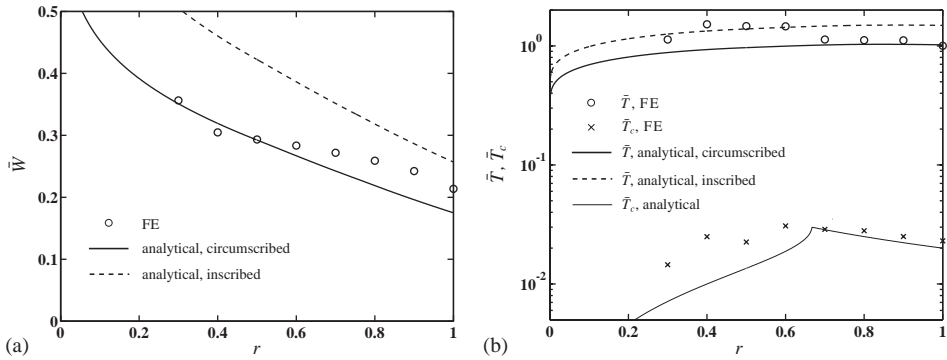


Fig. 11. Response of a clamped sandwich beam ($\bar{c} = 0.03, \bar{h} = 0.1$) with an isotropic core ($\bar{\rho} = 0.1, \bar{\sigma}_n = \bar{\sigma}_1 = 0.05, \varepsilon_D = 0.5$) subject to a total impulse $\bar{I}r = 0.002$. (a) The normalised deflection \tilde{W} , (b) structural response time \tilde{T} and core compression time \tilde{T}_c , as a function of patch loading size r . Analytical predictions employing the inscribing and circumscribing yield locus (for \tilde{W} and \tilde{T}) are included along with FE predictions.

value, and decreases with increasing r . However, for r less than about 0.7, the core is fully compressed ($\varepsilon_c = \varepsilon_D$) and \tilde{T}_c decreases with decreasing r (and increasing \bar{I}) according to Eq. (29).

4. Finite element study

Comparisons between the FE and analytical predictions of the response of the monolithic and sandwich beams are presented in this section. All computations were performed using the explicit time integration version of the commercially available FE code ABAQUS (version 6.3). The beams were modelled using four noded plane strain quadrilateral elements with reduced integration (element type *CPE4R* in the ABAQUS notation). Numerical damping associated with volumetric straining in ABAQUS explicit was switched off by setting the bulk viscosity associated with this damping to zero; using the default viscosity in ABAQUS results in substantial artificial viscous dissipation due to the large volumetric compression of the core. For a typical beam of geometry $\bar{c} = 0.03$ and $\bar{h} = 0.1$, there were 2 and 8 elements through the thickness of the face-sheets and core, respectively, and 100 elements along the beam span. Mesh sensitivity studies revealed that further refinements did not improve the accuracy of the calculations appreciably.

4.1. Constitutive description

Unless otherwise specified, the material properties of the sandwich beams are taken to be as follows. The face sheets of the sandwich beams are assumed to be made from an elastic ideally-plastic solid with yield strength σ_{fY} , a yield strain ε_{fY} and density ρ_f . The Young’s modulus is specified by $E_f \equiv \sigma_{fY}/\varepsilon_{fY}$. The solid is

modelled as a J2 flow theory solid. The core is modelled as a compressible continuum using the foam constitutive model of [Deshpande and Fleck \(2000\)](#). This constitutive law employs an isotropic yield surface specified by

$$\hat{\sigma} - \sigma_c = 0, \tag{46a}$$

where the equivalent stress is defined by

$$\hat{\sigma}^2 \equiv \frac{1}{1 + (\alpha/3)^2} [\sigma_e^2 + \alpha^2 \sigma_m^2]. \tag{46b}$$

Here, $\sigma_e \equiv \sqrt{3s_{ij}s_{ij}/2}$ is the von-Mises effective stress with s_{ij} the deviatoric stress tensor and $\sigma_m \equiv \sigma_{kk}/3$ the mean stress. The yield strength σ_c is specified as a function of the equivalent plastic strain using uniaxial compression stress versus strain data. Normality of plastic flow is assumed, and this implies that the ‘‘plastic Poisson’s ratio’’ $\nu_p = -\dot{\epsilon}_{22}^p/\dot{\epsilon}_{11}^p$ for uniaxial compression in the 1-direction is given by

$$\nu_p = \frac{1/2 - (\alpha/3)^2}{1 + (\alpha/3)^2}. \tag{47}$$

Numerical values for the reference material properties for the sandwich beam are taken to be as follows. The face-sheets are assumed to be made from a stainless steel of yield strength $\sigma_{fY} = 500$ MPa, yield strain $\epsilon_{fY} = 0.2\%$, elastic Poisson’s ratio $\nu = 0.3$ and density $\rho_f = 8000$ kg m⁻³. The strength of the core is taken to be representative of that for a lattice material such as the octet truss ([Deshpande et al., 2001](#)) made from the same solid material as the face sheets. Thus, the isotropic core yield strength is taken to be

$$\sigma_c = 0.5\bar{\rho}\sigma_{fY}, \tag{48}$$

where $\bar{\rho} \equiv \rho_c/\rho_f$ is the relative density of the core. The reference case is $\bar{\rho} = 0.1$ (i.e. core density $\rho_c = 800$ kg m⁻³) with $\alpha = 3/\sqrt{2}$ giving a plastic Poisson’s ratio $\nu_p = 0$. The plastic crush strength σ_c of the foam core is taken to be independent of the effective plastic strain up to a densification strain $\epsilon_D = 0.5$: beyond densification, a linear hardening behaviour is assumed with a very large tangent modulus $E_t = 0.2E_f$. Further, the core is taken to be elastically isotropic with a yield strain $\epsilon_{cY} = \sigma_c/E_f$ and an elastic Poisson’s ratio $\nu_c = 0$.

4.2. Monolithic beams

Consider a monolithic beam loaded with a spatially uniform pressure over the entire span of the beam. The pressure versus time history is specified by

$$p = \begin{cases} p_0 & \text{if } 0 \leq t \leq \tau, \\ 0 & \text{otherwise,} \end{cases} \tag{49}$$

such that the impulse $I = p_0\tau$. [Jones \(1989\)](#) and [Xue and Hutchinson \(2003\)](#) have shown that when $\bar{\tau} \equiv \tau/(L\sqrt{\rho_f/\sigma_{fY}}) < 0.01$, dynamic loading with a pressure versus

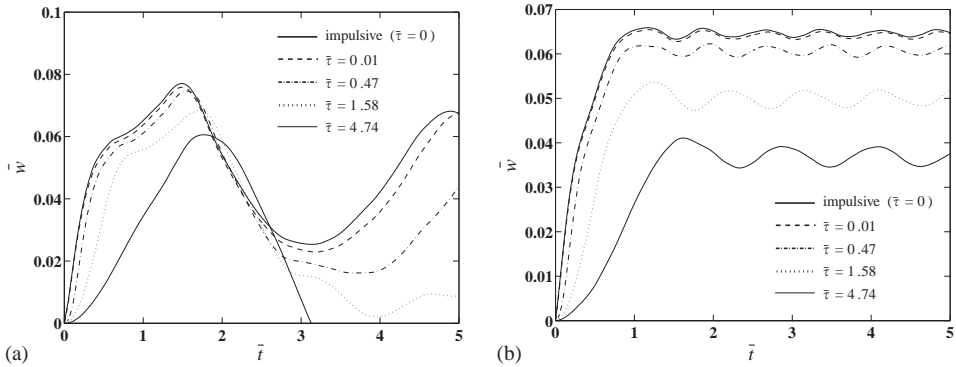


Fig. 12. Response of a monolithic beam ($\bar{H} = 0.02$) subject to a pressure versus time loadings ($r = 0.3$) corresponding to a normalised impulse $\bar{I} = 0.003$. The mid-span deflections are plotted as a function of time for two choices of the material yield strain (a) $\epsilon_{fY} = 0.2\%$ and (b) $\epsilon_{fY} = 0.02\%$.

time history $p(t)$ can be treated as impulsive with an impulse I . We proceed to verify this assumption for patch loaded beams.

Consider a monolithic beam with aspect ratio $\bar{H} = 0.02$ and made from an elastic ideally-plastic material. The beam is loaded over a central patch of size $r = 0.3$. The sensitivity of the normalised transverse displacement w/L at the mid-span to the ratio $\bar{\tau}$ is explored in Fig. 12 for a fixed impulse $\bar{I} = 0.003$. Each curve gives w/L as a function of normalised time $t/(L\sqrt{\rho_f/\sigma_{fY}})$, at selected values of $\bar{\tau}$. The limiting case of impulsive loading is included in Fig. 12: in the FE calculation the whole cross-section of the monolithic beam over the central section $r = 0.3$ is given a uniform initial velocity v_0 defined by

$$v_0 = \frac{\bar{I}}{\bar{H}} \sqrt{\frac{\sigma_{fY}}{\rho_f}}. \tag{50}$$

Fig. 12 includes the effect of the Young’s modulus E_f , with results for material yield strains $\epsilon_{fY} \equiv \sigma_{fY}/E_f = 0.2\%$ and 0.02% plotted in Figs. 12a and b, respectively. Intriguingly, elastic effects are seen to play an important role with significant elastic rebound for $\epsilon_{fY} = 0.2\%$ while only small elastic vibrations are seen for $\epsilon_{fY} = 0.02\%$. The maximum mid-span deflections are reasonably insensitive to the choice of ϵ_{fY} and for all practical purposes $\bar{\tau} < 0.01$ is equivalent to impulsive loading. This condition is satisfied in most practical shock loadings in air and water as discussed by Fleck and Deshpande (2004) and it thus suffices to model practical shock loadings as impulsive.

4.2.1. Comparison between finite element and analytical predictions

Consider a slender monolithic beam of thickness H and length $2L$ made from the same material as the face sheets of the reference sandwich beam; i.e. an elastic perfectly-plastic solid with a yield strength $\sigma_{fY} = 500$ MPa, yield strain $\epsilon_{fY} = 0.2\%$, an elastic Poisson’s ratio $\nu = 0.3$ and a material density $\rho_f = 8000$ kg m⁻³.

Comparisons between analytical and FE predictions for \bar{W} and \bar{T} are presented here. In the FE calculations \bar{W} is defined as the maximum mid-span deflection (i.e. the first peak in the w/L versus \bar{t} response in Fig. 12) and \bar{T} is the time at which the peak displacement is attained.

The comparisons are presented in three steps. First, consider a monolithic beam with aspect ratio $\bar{H} = 0.02$. Comparisons between FE and analytical predictions for the variations of \bar{W} and \bar{T} with \bar{I} are included in Figs. 4 and 5 for the choices $r = 0.3$ and 0.7 , respectively. FE predictions are shown for two choices of the material yield strain $\varepsilon_{fY} = 0.2\%$ and 0.02% . The yield strain is seen to have a negligible effect on \bar{W} and the FE calculations support the analytical predictions employing the circumscribing yield locus. In contrast, the FE calculations reveal that \bar{T} is sensitive to elastic effects for the choice $r = 0.3$. On the other hand, the magnitude of ε_{fY} has a negligible effect on \bar{T} for $r = 0.7$, and the analytical and FE results are in good agreement.

Second, consider the monolithic beam subject to a fixed impulse per unit area $\bar{I} = 0.003$ applied over patches $0 < r \leq 1$. Comparisons between FE and analytical predictions for \bar{W} and \bar{T} are shown in Figs. 6a and b, respectively: FE predictions for two choices of ε_{fY} are included in Fig. 6. The material yield strain ε_{fY} has a negligible effect upon \bar{W} and the FE predictions agree well with the analytical predictions employing the circumscribing yield locus. In contrast, the FE calculations predict that \bar{T} increases by about 40% when ε_{fY} is increased from 0.02% to 0.2% , for $r < 0.5$. Consistent with the results in Fig. 5, the degree of elasticity has a smaller influence on \bar{T} for $r > 0.5$. The FE predictions agree with the analytical predictions employing the circumscribing yield locus.

Third, compare FE and analytical predictions for the case of a fixed total impulse $\bar{I}r = 0.003$ applied over patches $0 < r \leq 1$. FE predictions of \bar{W} confirm the analytical predictions employing the circumscribing yield locus (Fig. 7a) with the predictions for $\varepsilon_{fY} = 0.2\%$ and 0.02% being almost equal. However, the FE predictions of \bar{T} are discontinuous at $r \approx 0.5$ with the predicted \bar{T} about 40% less at $r = 0.5^-$ compared to the value at $r = 0.5^+$ (Fig. 7b). The analytical calculations do not predict any discontinuity and the FE calculations only agree with the analytical predictions (circumscribing yield locus) for $r \geq 0.8$.

Overall, the above comparisons show that while the analytical model predicts \bar{W} with reasonable accuracy it only predicts \bar{T} accurately for $r > 0.5$. Typically, \bar{T} decreases with decreasing r and elastic effects are thought to play an important role in setting the structural response time in such cases. These effects are neglected in the analytical model which results in the discrepancies between the analytical and finite element results seen above.

4.3. Sandwich beams

Consider a representative sandwich beam with the reference material properties as specified above and geometry $\bar{c} = 0.03$ and $\bar{h} = 0.1$ subject to a spatially uniform pressure pulse over a central patch of size $r = 0.3$. The pressure versus time history is specified by Eq. (49) and selected value of \bar{I} are adopted, with $\bar{I} = 0.002$. Finite

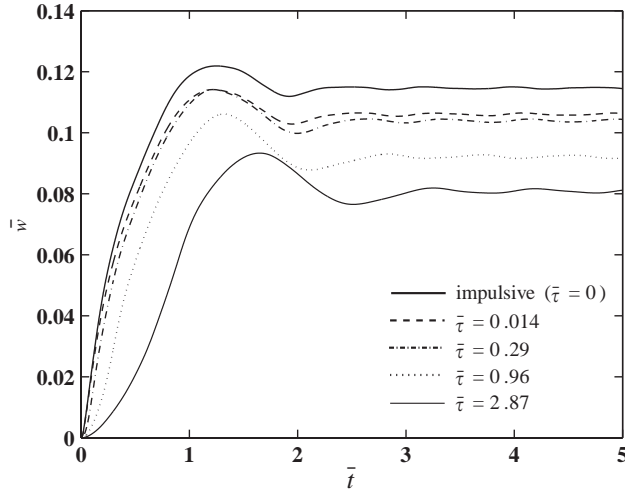


Fig. 13. Response of a sandwich beam ($\bar{c} = 0.03, \bar{h} = 0.1$) with reference material properties subject to a pressure versus time loadings ($r = 0.3$) corresponding to a normalised impulse $\bar{I} = 0.002$. The mid-span deflections of the rear face-sheet are plotted as a function of time.

element predictions of the normalised mid-span displacement of the rear face-sheet w/L is plotted in Fig. 13 as a function of the normalised time \bar{t} . The impulsive limit in which an initial velocity

$$v_0 = \frac{\bar{I}}{\bar{h}\bar{c}} \sqrt{\frac{\sigma_{fY}}{\rho_f}}, \tag{51}$$

is imparted to the front face-sheet is included in Fig. 13. Unlike the monolithic beam case, the sandwich beams ($\epsilon_{fY} = 0.2\%$) have negligible elastic rebound as plasticity in the core damps out the elastic vibrations. In line with the results of Qiu et al. (2003) for $r = 1$, we observe that the finite pressure loadings for $r = 0.3$ can be approximated as impulsive when $\bar{\tau} < 0.3$.

4.3.1. Comparison between finite element and analytical predictions

Comparisons between FE and analytical predictions are presented for a representative sandwich beam of geometry $\bar{h} = 0.1$ and $\bar{c} = 0.03$ and made from the reference materials. In particular, comparisons are presented for:

- (i) The maximum mid-span deflection \bar{W} of the rear face of the sandwich beam. This is defined as the peak in the displacement versus time trace.
- (ii) The structural response time T , defined as the time taken to reach this maximum deflection.
- (iii) Core compression ϵ_c , defined as the maximum nominal strain in the core at mid-span of the beam.

- (iv) Core compression time T_c , defined as the time taken to attain the core compression ϵ_c .

Comparisons between FE and analytical predictions of \bar{W} , \bar{T} and \bar{T}_c are given in Fig. 9 as a function of the impulse \bar{I} applied over a central patch of size $r = 0.3$. While the analytical predictions employing the inscribing yield surface capture the beam deflections reasonably accurately at low impulses, at higher impulses the analytical model employing the circumscribing yield locus is in better agreement with the FE predictions (Fig. 9a). The FE and analytical predictions for \bar{T} and \bar{T}_c are in good agreement (Fig. 9b); both the numerical and analytical predictions reveal that the core compression time is more than an order of magnitude smaller than the structural response time. Comparisons of the analytical and FE predictions for the core compression strain ϵ_c are included in Fig. 9a. The analytical calculations substantially over-predict ϵ_c for $\bar{I} > 0.0025$. This discrepancy can be rationalised by recalling that the analytical model neglects any momentum transfer away from the central loading patch during the core compression phase. With increasing \bar{I} the greater core compression gives rise to significant stretching of the front face sheet at the supports and thus to a drop in momentum. This effect is ignored in the analytical model and consequently the analytical model overpredicts ϵ_c at high values of \bar{I} . Comparisons between analytical and FE predictions of ϵ_c for $\bar{I} = 0.002$ are shown in Fig. 14. In line with the analytical predictions the FE results show that ϵ_c is independent of r . However, the analytical model again overpredicts the magnitude of ϵ_c .

Next consider the sandwich beam subject to a fixed value of impulse per unit area $\bar{I} = 0.002$. We investigate the response of the sandwich beam as a function of the

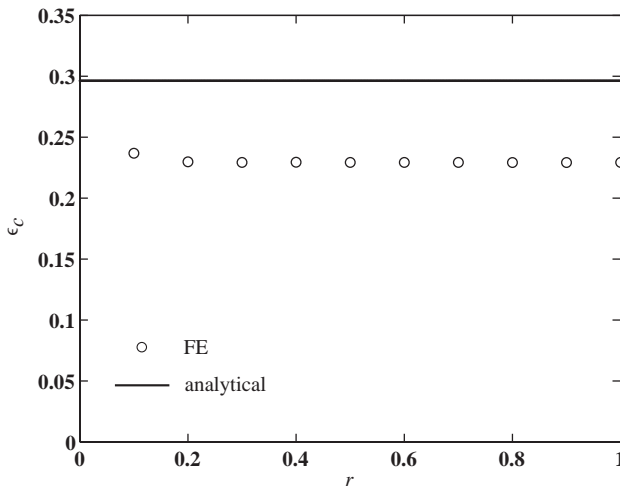


Fig. 14. The core compression strain ϵ_c as a function of loading patch size r for a clamped sandwich beam ($\bar{c} = 0.03$, $\bar{h} = 0.1$) with reference material properties, subject to an impulse per unit area $\bar{I} = 0.002$. Analytical predictions and FE predictions are included.

loading patch size r for $0 < r \leq 1$. Comparisons between the analytical and FE predictions for \bar{W} , \bar{T} and \bar{T}_c are shown in Fig. 10 and indicate good agreement between the FE and analytical predictions (circumscribing yield locus).

Comparisons between FE and analytical calculations for \bar{W} , \bar{T} and \bar{T}_c are shown in Fig. 11 for a fixed total impulse $\bar{I}r = 0.002$ as a function of the patch size r . Good agreement between the FE and analytical predictions (circumscribing yield locus) is seen for \bar{W} and \bar{T} . However, the analytical model under-predicts \bar{T}_c for $r < 0.6$. Both the analytical and FE calculations confirm that \bar{T}_c is less than \bar{T} by more than an order of magnitude, in support of the assumption that these phases can be decoupled.

5. Optimal design of sandwich beams

In the preceding section it has been demonstrated that the analytical formulae employing the circumscribing yield locus are in good agreement with FE calculations. We now employ the analytical finite deflection formulae to determine the optimal designs of sandwich beams that maximise the resistance of a sandwich beam of given mass to shock loading subject to the constraint of a maximum allowable rear face deflection. The optimisations are carried out with the assumption that the entire shock impulse is transmitted to the beam, representative for shock loadings in air (Fleck and Deshpande, 2004).

5.1. Core topologies

Over the last decade, a number of new core topologies for sandwich beams have emerged. Here we consider the six candidate core topologies (i) pyramidal core, (ii) prismatic diamond core, (iii) metal foam, (iv) square honeycombs, (v) hexagonal-honeycombs and (vi) an ideal core. Readers are referred to Fleck and Deshpande (2004) for a detailed discussion on the manufacturing route and properties of these cores. The relevant mechanical properties of the cores in terms of the normalised transverse compressive strength $\bar{\sigma}_n$ and longitudinal strength $\bar{\sigma}_l$ are listed in Table 1 as functions of the relative density $\bar{\rho}$ of the cores. It is worth mentioning that the

Table 1
Transverse and longitudinal strengths of the six sandwich core topologies investigated in this study

Core design	$\bar{\sigma}_n$	$\bar{\sigma}_l$
Pyramidal core	$0.5\bar{\rho}$	0
Metal foam core	$0.3\bar{\rho}^{3/2}$	$0.3\bar{\rho}^{3/2}$
Hexagonal-honeycomb core	$\bar{\rho}$	0
Square-honeycomb core	$\bar{\rho}$	$0.5\bar{\rho}$
Prismatic diamond core	$0.5\bar{\rho}$	$\bar{\rho}$
Ideal core	$\bar{\rho}$	$\bar{\rho}$

“ideal” core is 100% efficient in carrying load in both the transverse and longitudinal directions, though it is unclear whether such a core is physically realisable.

5.2. Minimum mass design

We restrict attention to cores made from same material as that of the face sheets in order to compare the performance of competing core concepts. The optimisations are conducted to maximise the resistance of a sandwich beam of a given mass to shock loadings subject to the constraint of a maximum allowable rear face deflection.

To help with this optimisation, it is instructive to construct a design chart relating the sandwich beam geometry to the shock impulse for a specified rear face-sheet deflection. Such a design chart for a normalised deflection $\bar{W} = 0.1$ of the pyramidal core ($\bar{\rho} = 0.1$) sandwich beams is plotted in Fig. 15 for $r = 0.3$. In order to give a conservative estimate of the shock resistance of these sandwich beams, we assume a densification strain $\epsilon_D = 1 - \bar{\rho}$. For the purposes of selecting sandwich beam geometries that maximise the blast impulse at a given mass, contours of non-dimensional mass \bar{m} have been added to Fig. 15 where

$$\bar{m} = \frac{m}{\rho_f L^2} = \bar{c}(2\bar{h} + \bar{\rho}), \tag{52}$$

and m is the mass per unit width of the sandwich beam. The arrows in Fig. 15 trace the optimum designs (designs that maximise \bar{I} for a given \bar{m}) with increasing mass. It is worth mentioning that the optimal designs have rather thick face-sheets (high \bar{h}). This indicates that the stretching effects dominate the response of these optimal clamped sandwich beams. Contours of the core compression strain ϵ_c are included in

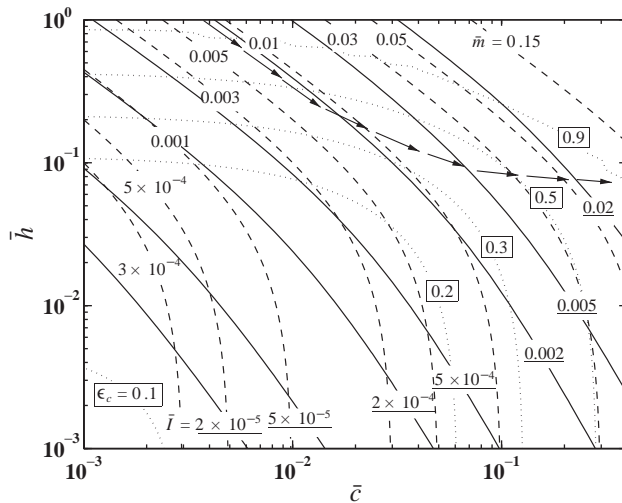


Fig. 15. Design chart for a sandwich beam ($r = 0.3$), with a pyramidal core ($\bar{\rho} = 0.1$, $\epsilon_D = 0.9$). The maximum mid-span deflection of the rear face-sheet is $\bar{W} = 0.1$. Contours of \bar{I} , \bar{m} and ϵ_c are displayed. The arrows trace the “optimal” designs with increasing mass \bar{m} .

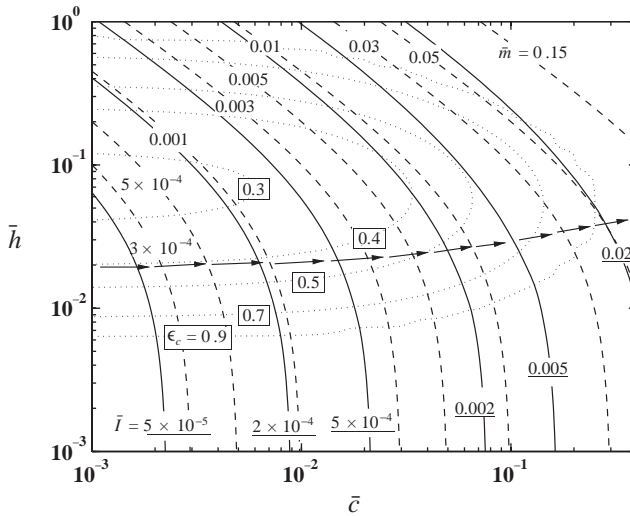


Fig. 16. Design chart for a sandwich beam ($r = 0.3$), with a prismatic diamond core ($\bar{\rho} = 0.1$, $\epsilon_D = 0.9$). The maximum mid-span deflection of the rear face-sheet is $\bar{W} = 0.1$. Contours of \bar{I} , \bar{m} and ϵ_c are displayed. The arrows trace the “optimal” designs with increasing mass \bar{m} .

the design chart: full core compression ($\epsilon_c = 1 - \bar{\rho} = 0.9$) only occurs at high values of \bar{c} and \bar{h} , with full core compression never being achieved in the optimal designs.

A similar design chart for the prismatic diamond core ($\bar{\rho} = 0.1$, $\epsilon_D = 1 - \bar{\rho}$) beams is plotted in Fig. 16 for $r = 0.3$. The chart differs from the pyramidal core chart of Fig. 16 in two ways: (i) the contours of \bar{I} are of similar shape to the \bar{m} contours and (ii) full core compression ($\epsilon_c = 0.9$) occurs for a larger fraction of the sandwich beam geometries in comparison to the pyramidal core sandwich beams. Both differences can be rationalised by noting that the shock resistance of the sandwich beams is dominated by the longitudinal stretching strength of the clamped beams. The prismatic diamond core with a longitudinal strength $\bar{\sigma}_1 = \bar{\rho}$ is 100% efficient in longitudinal stretching and thus the precise geometry of the sandwich beam at a given value of \bar{m} seems to play only a small role in determining its shock resistance. Arrows tracing the “optimal” designs of prismatic diamond core sandwich beams with increasing mass \bar{m} are shown in Fig. 16: it is worth emphasising that the shock resistance of the prismatic diamond core sandwich beams is only mildly sensitive to the (\bar{c}, \bar{h}) trajectory.

The shock resistance of the optimised sandwich beams is compared to that of monolithic beams in Fig. 17a for the choice $r = 0.3$. Specifically, the maximum sustainable impulse is plotted against the non-dimensional mass \bar{m} , with the deflection constraint $\bar{W} \leq 0.1$ imposed. In all cases the core relative density is taken as $\bar{\rho} = 0.1$ and the core densification strain fixed at $\epsilon_D = 1 - \bar{\rho}$. All sandwich beams outperform the monolithic beams; the ranking of core topologies in order of increasing shock resistance is metal foam, pyramidal core, hexagonal-honeycomb, square-honeycomb, prismatic diamond core and the ideal core. This order is the

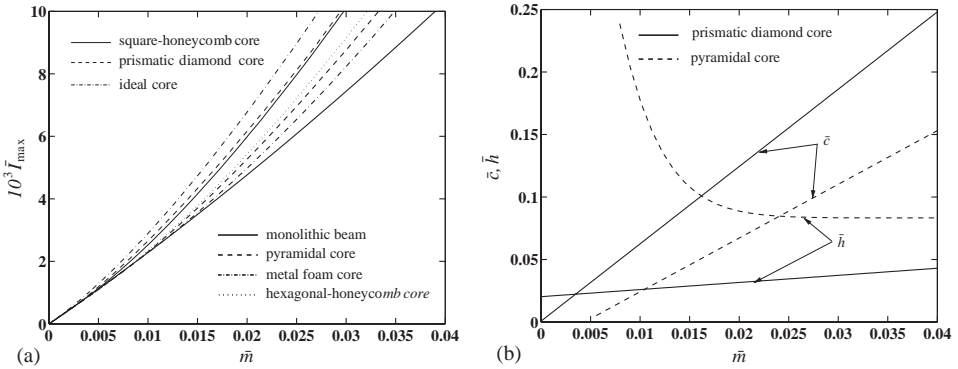


Fig. 17. (a) A comparison of the maximum shock impulse ($r = 0.3$) sustained by monolithic beams and by optimal designs of sandwich beams, subjected to the constraints $\bar{W} \leq 0.1$. (b) The corresponding optimal designs of sandwich beam with prismatic diamond and pyramidal cores. The core relative density is taken as $\bar{\rho} = 0.1$ and densification strain is $\varepsilon_D = 1 - \bar{\rho}$.

same as that noted previously by Fleck and Deshpande (2004) for the uniformly loaded ($r = 1$) sandwich beams. The geometries of the optimally designed sandwich beams are plotted in Fig. 17b for the prismatic diamond core and the pyramidal core.

5.2.1. Effect of the patch size r

In a practical shock loading event, the loading patch size is not expected to be known a priori and it is useful to explore the effect of loading patch size r on the optimal design of the sandwich beams.

The maximum shock impulses sustainable by sandwich beams with a pyramidal core and prismatic diamond core ($\bar{\rho} = 0.1, \varepsilon_D = 1 - \bar{\rho}$) subject to the constraint $\bar{W} \leq 0.1$, are plotted against \bar{m} in Fig. 18. Results are shown for the cases $r = 0.3$ and 1: as expected, the beams with $r = 0.3$ can sustain higher shock impulses per unit area. A comparison of the “optimal” designs for $r < 1$ obtained in this study with the optimal designs for $r = 1$ in Fleck and Deshpande (2004) reveals that the optimal designs of the sandwich beams are robust in the sense that they are nearly independent of the loading patch size r .

6. Concluding remarks

An analytical model has been derived for the response of clamped monolithic and sandwich beams subject to shock loading over a central patch. The predictions of the analytical model have been compared with dynamic FE calculations and the analytical model used to determine optimal designs of the sandwich beams. The main conclusions are:

1. The analytical model employing the circumscribing yield locus agrees well with the FE predictions. Elastic effects significantly affect the structural response times

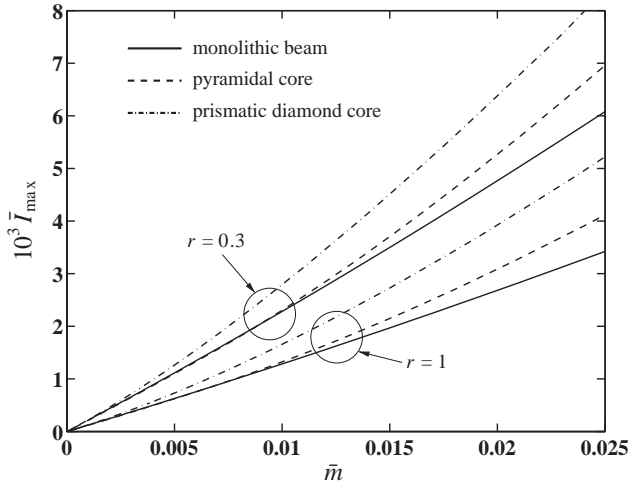


Fig. 18. A comparison of the maximum shock impulse sustained by the pyramidal and prismatic diamond core sandwich beams for $r = 0.3$ and 1.

of the monolithic beams for $r < 0.5$ but are seen to have a smaller influence on the structural response times of sandwich beams.

2. FE calculations demonstrate that the time scale for core compression separates from the time scale for bending/stretching of the sandwich beam, as assumed in the analytical model.
3. Optimal designs of sandwich beams can sustain larger shock impulses compared to monolithic beams of the same mass.
4. Prismatic core sandwich beams provide the maximum shock resistance due to the high longitudinal stretching resistance of the prismatic diamond core.
5. The optimal designs of the sandwich beams are not sensitive to the loading patch size r .

Acknowledgements

The authors are grateful to ONR for their financial support through US-ONR IFO grant number N00014-03-1-0283 on the The Science and Design of Blast Resistant Sandwich Structures. We are pleased to acknowledge Profs. A.G. Evans and J.W. Hutchinson for insightful discussions during the course of this work.

Appendix A. Approximate solution

Here we present a “modal” estimate for the deflection and structural response time of clamped monolithic and sandwich beams loaded over a central patch of size

$r \equiv a/L$. In the modal analysis we neglect the responses of the beams in phases I and II of the motion and consider only phase III. This permits us to obtain closed-form expressions for the response of the beam for the entire range $0 < r \leq 1$.

First consider the monolithic beam. The governing ODE for the modal solution is given by Eq. (10), for the choice of a circumscribing yield locus. The initial conditions are taken as

$$\bar{w}(0) = 0, \tag{A.1a}$$

$$\dot{\bar{w}}(0) = \frac{2\bar{I}r}{\bar{H}}, \tag{A.1b}$$

where the initial condition (A.1b) ensures that the momentum of the entire beam at time $t = 0$ is equal to the momentum imparted to the central patch of length $2a$. The solution of Eq. (10) with the above initial conditions gives

$$\bar{W} = \frac{\bar{H}}{2} \left(\sqrt{1 + \frac{16}{3} \frac{\bar{I}^2 r^2}{\bar{H}^4}} - 1 \right), \tag{A.2a}$$

and

$$\bar{T} = \frac{1}{\sqrt{3}} \tan^{-1} \left(\frac{4}{\sqrt{3}} \frac{\bar{I}r}{\bar{H}^2} \right). \tag{A.2b}$$

(Results for the choice of the inscribing yield locus can readily be obtained by replacing σ_{fY} by $0.618\sigma_{fY}$.)

Similarly, the modal solutions for the clamped sandwich beams are given by

$$\bar{W} = \alpha_1 \alpha_3 \left(\sqrt{1 + \frac{64}{3} \frac{\alpha_2^2}{\alpha_1^2} \bar{I}^2 r^2} - 1 \right) \tag{A.3a}$$

and

$$\bar{T} = \frac{1}{\sqrt{3}} \frac{1}{\alpha_2} \tan^{-1} \left(\frac{8}{\sqrt{3}} \frac{\alpha_2}{\alpha_1} \bar{I}r \right), \tag{A.3b}$$

for the choice of a circumscribing yield locus, where $(\alpha_1, \alpha_2, \alpha_3)$ are given by Eq. (39). Predictions employing the inscribing yield locus can readily be obtained by replacing σ_{fY} by $0.5\sigma_{fY}$.

References

Deshpande, V.S., Fleck, N.A., 2000. Isotropic constitutive models for metallic foams. *J. Mech. Phys. Solids* 48 (6–7), 1253–1283.
 Deshpande, V.S., Fleck, N.A., Ashby, M.F., 2001. Effective properties of the octet truss lattice material. *J. Mech. Phys. Solids* 49 (8), 1747–1769.
 Fleck, N.A., Deshpande, V.S., 2004. The resistance of clamped sandwich beams to shock loading. *J. Appl. Mech.* 71, 386–401.
 Jones, N., 1989. *Structural Impact*. Cambridge University Press, Cambridge.

- Li, Q.M., Jones, N., 1995. Blast loading of fully clamped beams with transverse shear effects. *Mech. Struct. Mach.* 23 (1), 59–86.
- Martin, J.B., Symmonds, P.S., 1966. Mode approximations for impulsively-loaded rigid-plastic structures. *J. Eng. Mech.: ASCE EM5*, 43–66.
- Qiu, X., Deshpande, V.S., Fleck, N.A., 2003. Finite Element analysis of the dynamic response of clamped sandwich beams subject to shock loading. *Eur. J. Mech. A: Solids* 22 (6), 801–814.
- Radford, D.D., Fleck, N.A., Deshpande, V.S., 2005. The response of clamped sandwich beams subject to shock loading. *Int. J. Impact Eng.*, to appear.
- Vashi, K.M., 1966. Effect of shear deformation in a beam impulsively loaded on a central portion, Master's thesis, Division of Engineering, Brown University, USA.
- Xue, Z., Hutchinson, J.W., 2003. A preliminary assessment of sandwich plates subject to blast loads. *Int. J. Mech. Sci.* 45, 687–705.
- Xue, Z., Hutchinson, J.W., 2004. A comparative study of blast-resistant metal sandwich plates. *Int. J. Impact Eng.* 30, 1283–1305.